

Fission-Fragment Mass Distribution and Particle Evaporation at low Energies *

CH. SCHMITT¹, J. BARTEL¹, K. POMORSKI^{1,2}, A. SUROWIEC²

¹*IR_eS – IN2P3/CNRS and Université Louis Pasteur, Strasbourg, France*

²*Katedra Fizyki Teoretycznej, Uniwersytet M. C. Skłodowskiej, Lublin, Poland*

Fusion-fission dynamics is investigated with a special emphasis on fusion reactions at low energy for which shell effects and pairing correlations can play a crucial role leading in particular to multi-modal fission. To follow the dynamical evolution of an excited and rotating nucleus we solve a 2-dimensional Langevin equation taking explicitly light-particle evaporation into account. The confrontation theory-experiment is demonstrated to give interesting information on the model presented, its qualities as well as its shortcomings.

PACS numbers: 21.60.Jz,21.10.Dr,21.10.-k,21.10.Pc

1. Introduction

The description of the dynamical evolution of a compound nucleus along its way to fission, i.e. from its rather compact ground-state shape to its scission configuration, represents an intricate problem. Many ingredients enter into the description of such a process, starting from a sufficiently precise account of the formation of the compound system, to the determination of the multi-dimensional energy landscape, to the coupling between the collective dynamics and the intrinsic degrees of freedom of the nucleus, to the concept used to describe light-particle evaporation which can occur all along the fission path. As a general microscopic treatment is completely out of scope, different theoretical approaches based on a more or less classical picture [1]-[6] have been proposed.

We have developed such a model describing the time evolution of a highly excited rotating nucleus and its subsequent decay through symmetric fission with pre-fission light-particle emission [5]. The aim of the present

* This paper is devoted to Professor Adam Sobiczewski on the occasion of his 70th birthday

paper is to extend our theory to lower energy. Through a comparison with the available experimental data, in particular fission-fragment mass distributions and neutron pre-scission multiplicities, we hope to get some valuable information on the behavior of transport coefficients at low energy.

2. Evolution of an excited rotating nucleus towards fission

To study the time evolution of an excited rotating nucleus, the system is assumed to follow a stochastic Langevin equation of motion [7] of one or several collective variables that describe in an appropriate and sufficiently flexible way the deformation of the nucleus along its path to fission .

2.1. Description of nuclear shapes

To describe the large variety of deformed shapes that can appear in the fission process, the Trentalange–Koonin–Sierk (TKS) nuclear shape parametrization [8] is used. In the case of an axially symmetric system the nuclear surface is given by

$$\rho_s^2(z) = R_0^2 \sum_{\ell=0}^{\Lambda} \alpha_{\ell} P_{\ell} \left(\frac{z - \bar{z}}{z_0} \right) = R_0^2 \sum_{\ell=0}^{\Lambda} \alpha_{\ell} P_{\ell}(u), \quad z_0 = \frac{2R_0}{3\alpha_0}, \quad u = \frac{z - \bar{z}}{z_0} \quad (1)$$

with $2z_0$ the elongation of the shape in z direction, \bar{z} its geometrical center and R_0 the radius of the corresponding spherical nucleus. The deformation parameters α_{ℓ} define the shape.

This parametrization is strongly related to the well known Funny Hills $\{c, h, \alpha\}$ parametrization [9] recalled below :

$$\rho_s^2(z) = c^2 R_0^2 \begin{cases} (1 - u^2)(A + \alpha u + B u^2), & B \geq 0 \\ (1 - u^2)(A + \alpha u) \exp(B c^3 u^2), & B < 0 \end{cases} \quad (2)$$

with $z_0 = c R_0$ and where A and B are related to c and h through

$$A = \frac{1}{c^3} - \frac{1}{5}B, \quad B = 2h + \frac{1}{2}(c - 1).$$

We have tested the convergence of these parametrizations for the description of symmetric fission-barrier heights and compared it to the results obtained using the expansion of the nuclear surface in spherical harmonics. The agreement with experiment was better with the TKS parametrization using 3 parameters α_2 , α_4 , α_6 than with the later including deformation parameters up to β_{14} , thus showing the fast convergence of the TKS parametrization.

2.2. Fission dynamics and Langevin equation

Fission dynamics is investigated through the resolution of the Langevin equation which for the generalized coordinates q_i is given by

$$\begin{aligned} \frac{dq_i}{dt} &= \sum_j [M^{-1}(\vec{q})]_{ij} p_j \quad (3) \\ \frac{dp_i}{dt} &= -\frac{1}{2} \sum_{j,k} \frac{d[M^{-1}(\vec{q})]_{jk}}{dq_i} p_j p_k - \frac{dV(\vec{q})}{dq_i} - \sum_{j,k} \gamma_{ij}(\vec{q}) [M^{-1}(\vec{q})]_{jk} p_k + F_i(t) \end{aligned}$$

where p_i are the canonical momenta associated with the coordinates q_i . $[M(\vec{q})]$ represents the tensor of inertia determined in our approach in the irrotational incompressible fluid approximation of Werner-Wheeler as developed by Davies, Sierk and Nix [10] and $[\gamma(\vec{q})]$ corresponds to the friction tensor calculated in the framework of the so-called *wall and window friction* model [11, 12]. The collective potential $V(\vec{q})$ is defined in our approach as the Helmholtz free energy at given deformation [5, 13]. The term $F_i(t)$ stands for the random Langevin force which couples collective dynamics to the intrinsic degrees of freedom. We have $F_i(t) = \sum_j g_{ij}(\vec{q}) G_j(t)$ where the strength tensor $[g(\vec{q})]$ is given by the diffusion tensor $[D(\vec{q})]$ through $D_{ij} = \sum_k g_{ik} g_{jk}$ and $\vec{G}(t)$ is a stochastic function. In our model it is assumed that diffusion is related to friction through the Einstein relation $[D(\vec{q})] = [\gamma(\vec{q})] T$ where T corresponds to the nuclear temperature [5]. The explicit expressions of these quantities in the TKS parametrization have been presented and discussed in details in [13].

The friction model we are using is based on a classical concept valid at high energy. When going to lower temperatures this picture can only be considered as an upper limit since nucleon-nucleon collisions become less and less frequent thus reducing friction [14]. We also know that the Einstein relation is in principle only valid at high energy [15]. We shall come back to these approximations in section 4.5. and show that one has to modify this simplified description at low temperature to correctly describe the experimental data.

Another quantity entering the Langevin equation and whose temperature dependence requires special attention is the potential $V(\vec{q})$ namely because of the vanishing of quantal effects at high excitation energy. In our approach valid up to now for symmetric fission, it consisted of a temperature dependent Liquid Drop Model (LDM) term only. At lower energy we have to add to this macroscopic contribution the shell corrections which are evaluated at each deformation using the Strutinsky's approach [16] and the pairing correlations which we calculate in the framework of the BCS model [17] with a constant pairing strength (*seniority scheme*) [18].

The generalized coordinates q_i which enter the Langevin equation are either chosen as the deformation parameters generating the nuclear shape (e.g. coefficients α_ℓ) or as more physically relevant quantities (elongation, mass asymmetry, etc) which are determined through these parameters [13].

Up to now [5, 19] we have investigated the case of highly excited compound nuclei giving rise to symmetric fission. Such a process can be described approximately by a single collective coordinate characterizing the nuclear elongation as explained in ref. [13]. This approach has been proven quite successful reproducing experimental pre-scission neutron multiplicities with an accuracy of 10 – 20% for nuclei ranging from ^{126}Ba to the region of superheavy elements [19]. As our aim in the present paper is to investigate systems at lower energy, one has to be able to describe *multi-modal* fission caused by the competition between symmetric and asymmetric splitting generated by the quantal effects present at low temperature. Dealing with asymmetric shapes, we need to take at least two collective variables (e.g. elongation and asymmetry) into account describing the compound nucleus along its deformation process. For this purpose we choose to use the Funny-Hills parametrization and to restrict ourselves to the 2-dimensional (c, α) deformation space imposing $h = 0$. Indeed, one can show that the influence of the *neck parameter* h can be considered as rather small, at least in the semi-classical limit [20, 21].

2.3. Entrance channel effects

In order to solve the Langevin equation of motion one needs to specify the initial conditions of the trajectory (for reasonable statistics we need to consider 10^4 to 10^6 trajectories) from which the compound system starts and evolves either through the fission channel or ending up as an evaporation residue. The initial conditions for \vec{q}_0 and \vec{p}_0 are fixed to the ground-state deformation and drawn from a normalized gaussian distribution respectively [5]. The nuclear systems we have investigated so far were generated through heavy-ion collisions which can lead to a large variety of the angular momentum of the synthesized nucleus. The initial spin distribution of the former is determined in our model by solving a Langevin equation [3] describing the evolution of the two colliding ions from an infinite distance up to fusion. The Langevin equation (3) is then solved in order to describe the dynamical evolution of the synthesized nucleus taking particle emission into account by coupling the Langevin equation to the Master equations governing this evaporation process. For each trajectory we start with a given compound system characterized by its excitation energy and angular momentum. The final prediction, which can be compared to experiment, is then determined by weighting the calculations made at given angular momentum by the fusion-fission cross section [19].

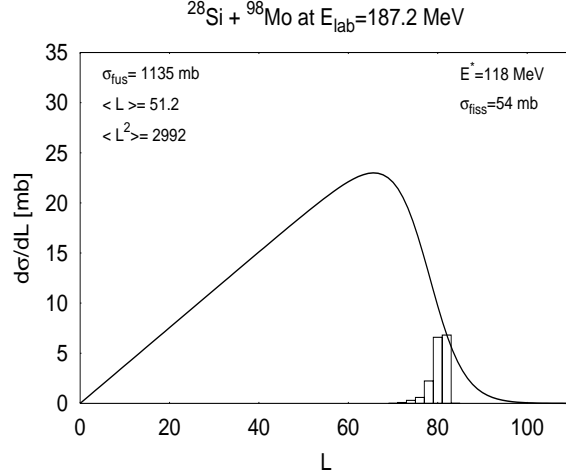


FIG. 1. Differential fusion (solid line) and fission (histogram) cross-section for the reaction $^{28}\text{Si} + ^{98}\text{Mo} \rightarrow ^{126}\text{Ba}$ at $E_{tot}^* = 118.5$ MeV.

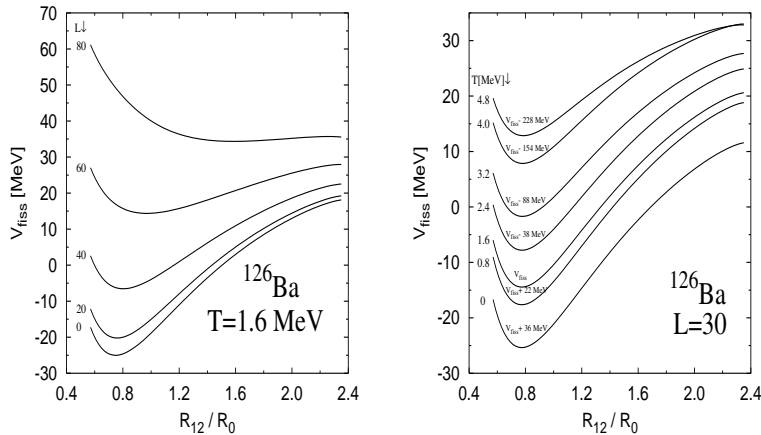


FIG. 2. Fission barriers for the nucleus ^{126}Ba as function of angular momentum at fixed total excitation energy (left) and of temperature at fixed angular momentum (right).

Fig. 1 shows the fusion and fission cross-sections obtained for the system $^{28}\text{Si} + ^{98}\text{Mo} \rightarrow ^{126}\text{Ba}$ at a total excitation energy of $E_{tot}^* = 118.5$ MeV. One notices that fission yields are rather small and located in the tail of the spin distribution at high values of the angular momentum where fission barriers are low. A study of the fission-barrier height as function of angular momentum and thermal excitation energy is given in Fig. 2 from which we conclude that a careful description of the fusion cross-section through its initial spin distribution is necessary if one wants to describe the competition between the decay by fission and light-particle evaporation.

3. Light-particle emission

Fission dynamics of an excited rotating nucleus usually goes along with the emission of light particles (we will consider neutrons, protons and α particles). This evaporation process is governed by the emission width $\Gamma_\nu^{\mu\kappa}(E^*, L)$ for emitting a particle of type ν , energy ε_μ and angular momentum ℓ_κ from a nucleus characterized by its thermal excitation energy E^* and its rotational angular momentum L . In order to determine $\Gamma_\nu^{\mu\kappa}(E^*, L)$ we use two different prescriptions.

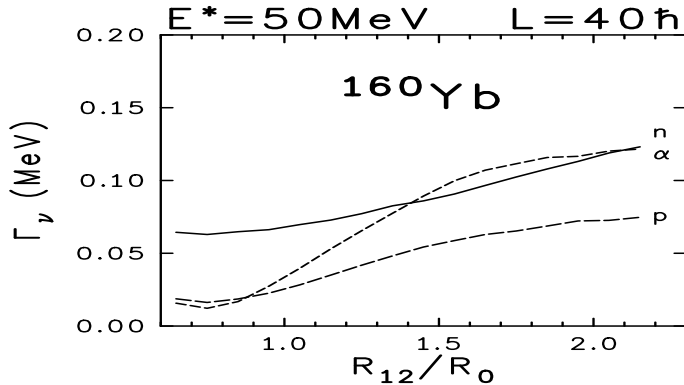


FIG. 3. Emission widths for neutrons, protons and α particles emitted from the system ^{160}Yb ($E^*=50$ MeV, $L=40\hbar$) as a function of elongation.

In Weisskopf's evaporation theory [22] the decay rates are essentially evaluated through the level densities of the mother and the daughter nuclei and the transmission coefficient for emitting the particle from a given point of the nuclear surface into a given direction as explained in ref. [5]. In practice it is not possible to discuss the values of the emission width for each energy, angular momentum and position of the emission point on the nuclear surface. We therefore use them to determine the probability $\Gamma_\nu(E^*, L)$ of emitting a given particle from a given nucleus at given deformation. This simplified procedure calculates a transmission coefficient obtained by an averaging over the different emission directions and over the whole surface of the deformed nucleus. A detailed description of this procedure can be found in ref. [5]. Also other groups [2, 4, 6] have dealt with particle emission in connection with fission dynamics but, to our knowledge, none of them has taken nuclear deformation explicitly into account as we have, even if it is in an approximate way. In Fig. 3 the evaporation rate Γ_ν is displayed for a hot rotating nucleus ^{160}Yb . It becomes obvious that the deformation dependence of Γ_ν is essential and that assuming a deformation independent emission width could probably lead to wrong predictions.

The second approach we used so far to describe particle emission calculates the transition rates $\Gamma_\nu^{\mu\kappa}$ through the probability that a particle which impinges on the nuclear surface at a given point \vec{r}_0' and with a given velocity \vec{v}_0' is actually transmitted [23]. In this framework the quantity $\Gamma_\nu^{\mu\kappa}$ is determined as

$$\Gamma_\nu^{\mu\kappa} = \frac{d^2 n_\nu}{d\varepsilon_\mu d\ell_\kappa} \Delta\varepsilon \Delta\ell. \quad (3)$$

The number n_ν of particles of type ν which are emitted per time unit through the surface S of the fissioning nucleus is given by

$$n_\nu = \int_S d\sigma \int d^3 p' f_\nu(\vec{r}_0', \vec{p}') v'_\perp(\vec{r}_0') w_\nu(v'_\perp(\vec{r}_0'))$$

where the quantity $f_\nu(\vec{r}', \vec{p}')$ corresponds to the quasi-classical phase-space distribution function [23].

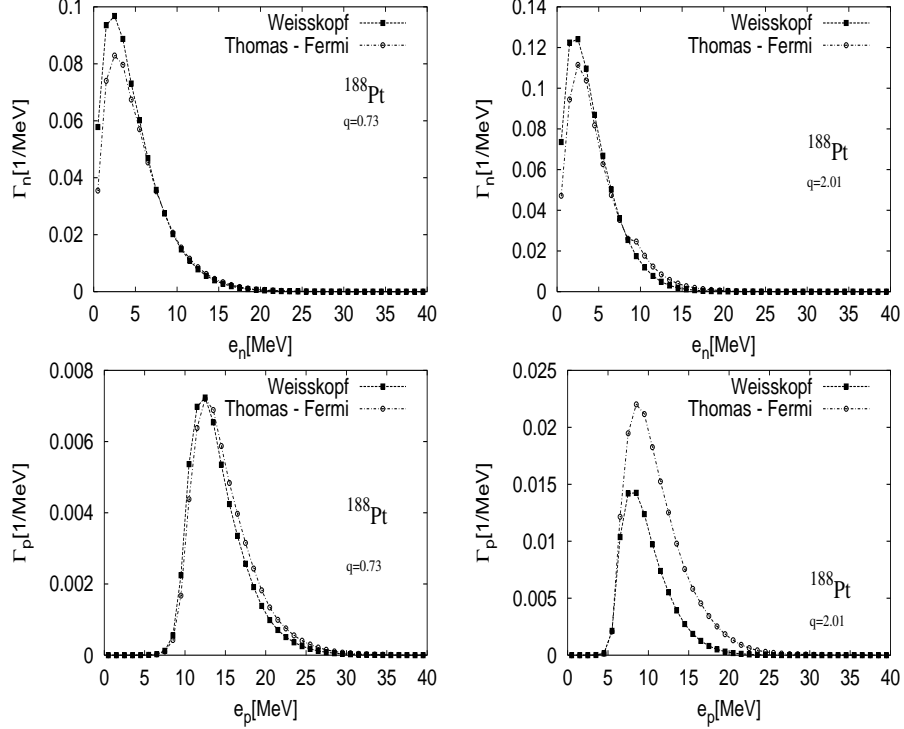


FIG. 4. Emission rates Γ_n and Γ_p for neutrons and protons obtained in the Weisskopf and the distribution function (called Thomas-Fermi here) approaches at deformations close to the spherical shape ($q = 0.73$) and to the scission configuration ($q = 2.01$).

Fig. 4 gives a comparison of the neutron and proton emission rates in the two evaporation models obtained for different values of a collective coordinate q related to nuclear elongation [13] for the system ^{188}Pt ($E^*=100$ MeV, $L=0\hbar$) [24]. Both models yield emission rates that are reasonably close for both types of particles for all elongations except for an increase of the distribution function approach relative to the Weisskopf prediction in the case of protons for very large deformations. One should also notice the deformation dependence of the proton emission width Γ_p that can be easily understood if one keeps in mind that the Coulomb barrier which charged particles have to overcome depends on the direction of the emission (an emission along the tips is favored compared to an emission perpendicular to the symmetry axis).

The determination of the phase-space distribution function is quite intricate in the case of α -particles which are composite particles. We are presently working on a model which determines the α -particle distribution function f_α through those of two correlated protons and neutrons respectively [24].

4. Theoretical results of fission dynamics

4.1. Influence of quantal effects

4.1.1. One- versus 2-dimensional Langevin equation

In the framework of the 2-dimensional Langevin equation solved in the (c, α) deformation space, the LDM energy landscape is displayed on Fig. 5 together with a typical fission trajectory for the compound nucleus ^{227}Pa at a total excitation energy of $E_{tot}^*=26$ MeV and an angular momentum of $L = 60\hbar$. We choose this specific nuclear system because it was the object of a recent experimental campaign [21]. As no shell effects are taken into account here, only the symmetric fission valley is present. Consequently the compound nucleus starting from its ground-state deformation ($c=1.11, \alpha=0$), naturally ends up in the symmetric fission channel. In this calculation we have not coupled particle emission to the Langevin equation and therefore cannot make any statement on particle multiplicities. The fission time, defined as the average time which a trajectory takes to reach the scission point, is in the present 2-dimensional treatment reduced by about 7% ($5.96 \cdot 10^{-17}$ sec versus $6.36 \cdot 10^{-17}$ sec) as compared to its 1-dimensional value [20].

Let us try to understand this result since it might seem astonishing that resolving the 2-dimensional Langevin equation, where trajectories can fill out more effectively the deformation space (as it is demonstrated with the typical trajectory drawn on Fig. 5), would lead to shorter fission times than when the compound nucleus follows the deepest symmetric fission valley of the 1-dimensional picture. In fact we have to think of the Langevin equation

as an approximation to the Fokker-Planck one which deals with probability distributions. In an 1-dimensional space the system is constrained whereas, the more the dimensionality is increased, the less constraints one has.

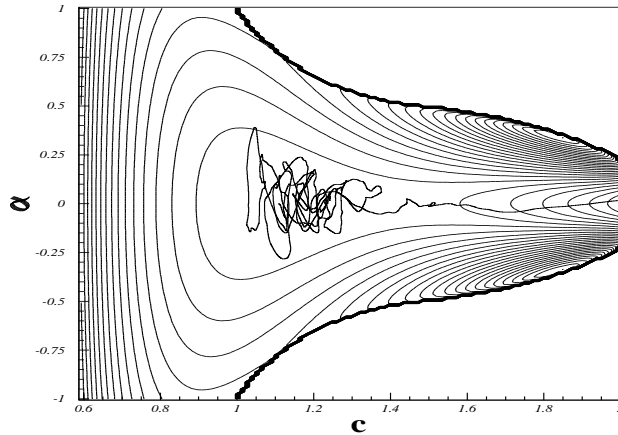


FIG. 5. Temperature dependent LDM energy landscape and typical fission trajectory for the compound system ^{227}Pa ($E_{tot}^* = 26$ MeV, $L = 60\hbar$).

This result on fission times seems also to indicate that in the case of highly excited nuclei our previous 1-dimensional description was already fairly accurate. The small change in times should indeed imply a rather small change in pre-fission particle multiplicities.

4.1.2. Influence of shell effects and pairing correlations

Let us now go one step further by including in our potential energy calculation quantal effects and their dependence on temperature. It is generally admitted that shell corrections have disappeared for temperatures above 2.5 to 3 MeV whereas pairing correlations have already vanished at $T \approx 1.5$ MeV or even before. In order to take care of the T -dependence of quantal corrections we multiply their values obtained at $T=0$ MeV with a temperature smoothing function which goes to zero at $T=3$ MeV for shell corrections and at $T=1.5$ MeV in the case of pairing [25] - [28]. The energy landscape then obtained for $E_{tot}^* = 26$ MeV and $L = 60\hbar$ is drawn on Fig. 6. Comparing the landscapes in Figs. 5 and 6, one notices the appearance, due to the presence of microscopic corrections, of asymmetric fission channels beyond $c \approx 1.7$ ending up in well pronounced valleys around $\alpha \approx \pm 0.035$.

The resolution of the Langevin equation in the landscapes of Figs. 5 and 6 gives rise to the distributions for the asymmetry parameter and fission-fragment masses presented in Figs. 7 and 8 respectively. Whereas symmetric distributions were obviously expected for the pure LDM landscape, the distributions obtained in the case where quantal effects are present are a little

surprising, because of their very strong asymmetry in spite of the rather flat energy landscape of Fig. 6 in the asymmetry direction α for large elongations ($c \approx 2.0$). However one should not forget that the fragment mass distribution is decided all along the fission path and not only in the immediate neighborhood of the exit point [29] - [31]. As the asymmetric valley is around 1 MeV deeper than the symmetric fission path in the vicinity of $c \approx 1.8 - 1.9$ where $\alpha \approx \pm 0.035$, the predominant part of the trajectories finally ends up in this asymmetric channel.

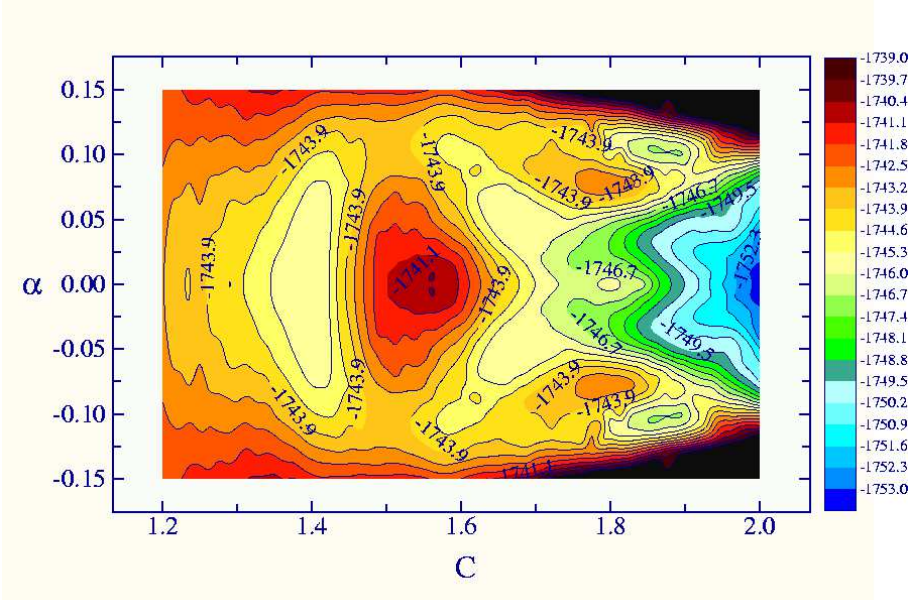


FIG. 6. Same as Fig. 5 but with inclusion of quantal effects.

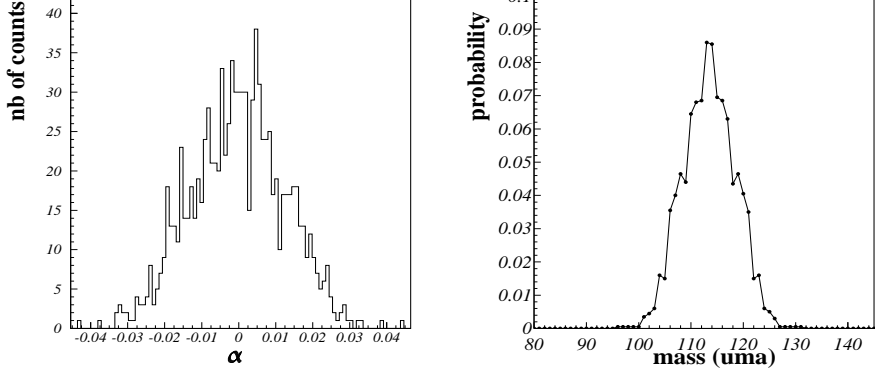


FIG. 7. Fission-fragment distribution as function of the asymmetry parameter α (left) and of the fragment mass (right) when quantal effects are omitted.

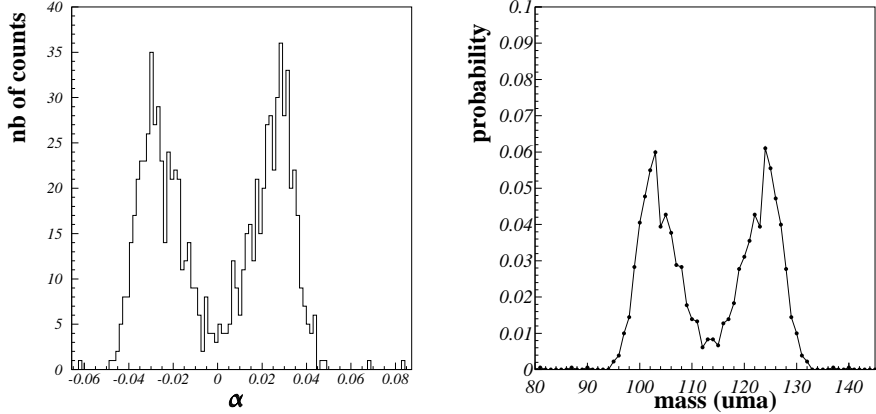


FIG. 8. Same as Fig. 7 but with inclusion of quantal effects.

It is interesting to notice that the average fission time is increased from $8.0 \cdot 10^{-17}$ sec to $16.2 \cdot 10^{-17}$ sec when going from the LDM picture to the one with shell and pairing corrections.

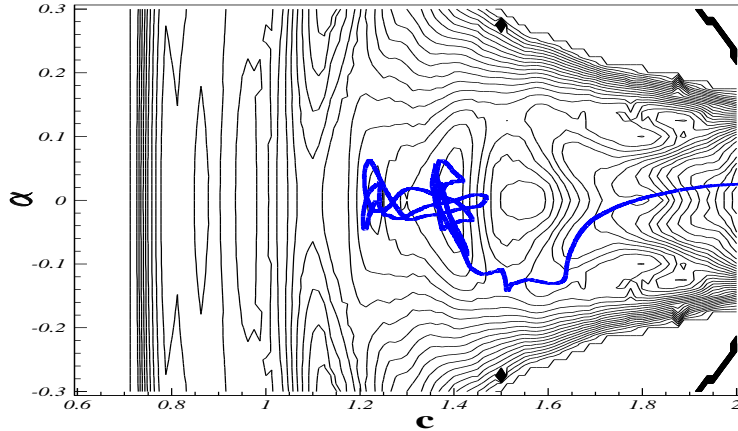


FIG. 9. Same as Fig. 6 with a typical asymmetric fission trajectory.

In the LDM landscape the symmetric fission barrier at $L = 60$ MeV is of the order of 0.7 MeV. On the other hand when quantal effects are included, the asymmetric fragment partition related to $\alpha \approx \pm 0.035$ corresponds to a barrier of 0.1 MeV. One notices that in spite of a lower barrier height when including microscopic corrections the corresponding fission time is larger than in the semi-classical picture. One understands this result if we compare the typical symmetric trajectory drawn on Fig. 5 to the typical asymmetric trajectory drawn on Fig. 9. In the former case the system cannot overcome the rather high *mountain top* at $c \approx 1.55$ for $\alpha \in [-0.06, 0.06]$

and consequently has to bypass it along $\alpha \approx \pm 0.1$ before reaching the asymmetric valley for $\alpha \approx \pm 0.035$. One could say that the path is *longer*. Let us note that a small energy difference (of the order of a few hundreds keV) between valleys can lead to very different fragment distributions what suggests the strong dependence of the dynamics on the *details* of the energy landscape. This drastic sensitivity to the structure of the landscape requires to be careful when one performs energy calculations in the deformation space.

4.2. Dynamics including light-particle evaporation

Even if we know that particle evaporation is strongly reduced at low energy we have to admit that we do not have yet a complete description evaluating the emission widths Γ_ν at low temperature since one can seriously question the validity of the Weisskopf's theory at such energies and since our development of the more microscopic phase-space distribution function approach is not complete. Nevertheless in order to investigate particle evaporation, we consider in this section the compound nucleus ^{227}Pa at a higher total excitation energy of 56 MeV for which we believe that the Weisskopf's approach should be approximately valid.

	V^{LDM}	$V^{LDM} + \delta E$
$\sigma_{fis}/\sigma_{tot} (\%)$	99.8	98.5
$\bar{t}_{fis} (\times 10^{-17} \text{ sec})$	2.335	3.275
M_n	1.806	2.153
M_p	0.010	0.006
M_α	0.017	0.011

Table 1 : Influence of quantal corrections on fission probability, average fission time and light-particle multiplicities obtained for the system ^{227}Pa ($E_{tot}^* = 56$ MeV, $L = 60\hbar$).

In Table 1 we compare the fission cross section, average fission time and light-particle multiplicities obtained for the pure LDM description to the ones related to the potential energy surface including shell and pairing corrections. As in the case without particle evaporation, one observes an increase of the fission time when quantal effects are taken into account. Whereas the neutron pre-scission multiplicity is larger in the calculations with microscopic corrections, charged particle multiplicities are smaller. With Fig. 3 we have seen that neutrons can be emitted whatever the nuclear elongation, i.e. all along the fission path, and that their emission probability increases with increasing deformation. A longer fission time should therefore lead to a larger neutron multiplicity. Charged particles are preferentially

emitted at large deformations (see again Fig. 3). One has, however, to remember that when charged particle emission is favored a substantial amount of the available excitation energy of the emitting nucleus can already have been carried away through neutron emission. In addition one finds that the gradient of the potential energy for the asymmetric fission path including quantal effects is larger between saddle and scission points than the one of the symmetric valley of the LDM landscape. This suggests that the corresponding time scale for the descent from saddle to scission is smaller in the case when shell and pairing effects are present what again favors a reduction of charged particle multiplicities.

4.3. Influence of excitation energy and angular momentum

As shown in Fig. 10 an increase of the total excitation energy of the system from 26 to 56 MeV (which for a given angular momentum $L = 60\hbar$ implies an increase of the thermal excitation energy) leads to a larger contribution to the symmetric fission mode. This result is obviously due to the vanishing of quantal effects when the nuclear temperature increases. However it can also be partly explained by a larger diffusion generated by the larger temperature (see Einstein relation). The corresponding larger oscillations thus allow the nucleus to *explore more easily* the energy landscape being able to overcome higher barriers and consequently to pass from one valley to another instead of being trapped preferentially in the deepest valley (which is asymmetric for the system presently considered). In ref [21] we also investigated the impact of the angular momentum on fission dynamics and obtained an relative increase of the symmetric fission cross section for increasing angular momentum due to a decrease of the fission barrier height.

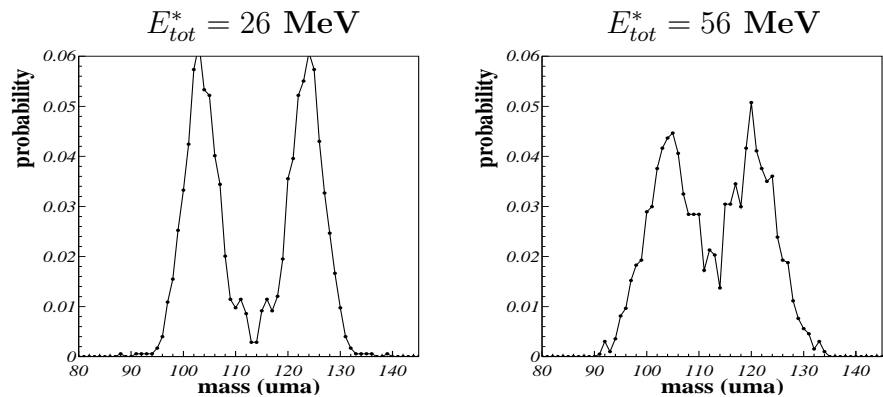


FIG. 10. Fission-fragment mass distributions for two different values of the total excitation energy of the compound nucleus ^{227}Pa at an angular momentum of $L = 60\hbar$.

4.4. Evaluation of shell corrections close to the scission point

In the framework of the Strutinsky method, shell correction calculations need to determine nuclear single particle levels which in our approach are the eigenvectors of a deformed Saxon Woods potential of standard parametrization [9]. In practice these states are obtained by an expansion in the basis of a deformed harmonic oscillator. This oscillator basis is an *one-center* basis which is probably not so well adapted if one is interested in describing shapes near the scission point. Indeed, for such strongly elongated and possibly *necked-in* surfaces, a *two-center* basis seems to be more adapted taking the structure of the nascent fragments better into account. We stress this technical detail in order to focus on the importance of a careful determination of shell effects at very large deformations. To illustrate this point we compare on Fig. 11 the fragment mass distribution obtained when the dynamical calculation is artificially stopped at an elongation $c_{scis} = 1.8$ to the one obtained when this calculation is carried through up to the geometrical scission point $c_{scis} = c_{geo}$ where the splitting into two fragments takes place. The broad distribution related to $c_{scis} = 1.8$ can be easily understood with Fig. 6 where the quite flat potential landscape in the α direction around $c \approx 1.8$ can give rise to a large variety of mass partitions. In spite of this, the final distribution at c_{geo} is rather strongly asymmetric. Moreover the value $c = 1.8$ corresponds to a quite important elongation, i.e. an elongation for which one can already have a reasonable idea of the asymmetry of the nascent fission fragments [31]. The present investigation points out the importance of quantal effects for $c > 1.8$ and with it the necessity of their accurate determination for these largest deformations. To avoid problems related to the choice of this one-center basis we perform the diagonalisation taking a very large number of basis states into account.

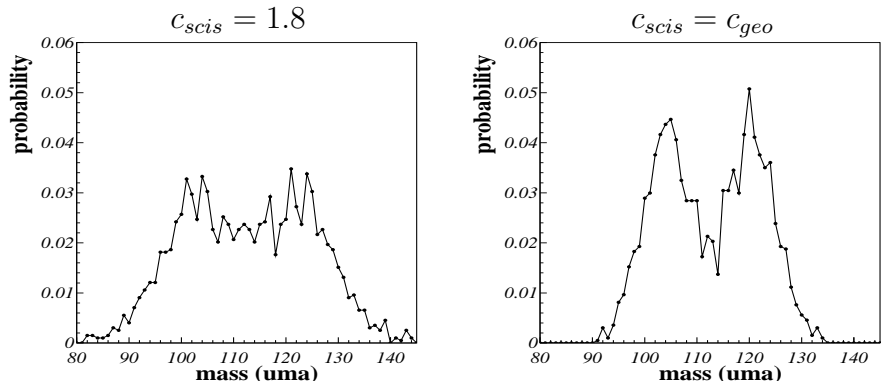


FIG. 11. Fission-fragment mass distributions obtained for the system ^{227}Pa ($E_{tot}^* = 56$ MeV, $L = 60\hbar$) for $c_{scis} = 1.8$ and $c_{scis} = c_{geo}$ (see text).

4.5. Temperature dependence of transport coefficients

As mentioned in section 2.2. we probably overestimate friction at low temperature. As demonstrated on Fig. 12 the reduction of friction by a factor of two ($0.5 w\&w$) results in a striking difference as compared to the full wall-and-window friction ($w\&w$). A larger friction causes a decrease of the kinetic energy of the system which is therefore more sensitive to the *fine structure* of the landscape and consequently is more easily trapped in the deepest valleys. A smaller friction, on the contrary, allows the system, with larger kinetic energy, to move more freely through the landscape, to overcome more easily eventual barriers, resulting in a broader distribution. Reducing friction by a constant factor is obviously an extremely crude approximation to a real temperature dependent viscosity. We use this picture here simply to investigate the influence of friction on fragment distributions and light-particle multiplicities.

The procedure used in order to simulate in an approximate way the vanishing of quantal effects with temperature (see section 4.1.2) is still nowadays subject of controversies, in particular what pairing is concerned [25] - [28]. Our investigations dealing with this point (for details see ref [21]) showed that the T-dependence of shell and pairing corrections cannot be neglected, even if our system is already in the beginning of its decay at quite low excitation energy, which can still decrease along the fission path (namely due to particle evaporation).

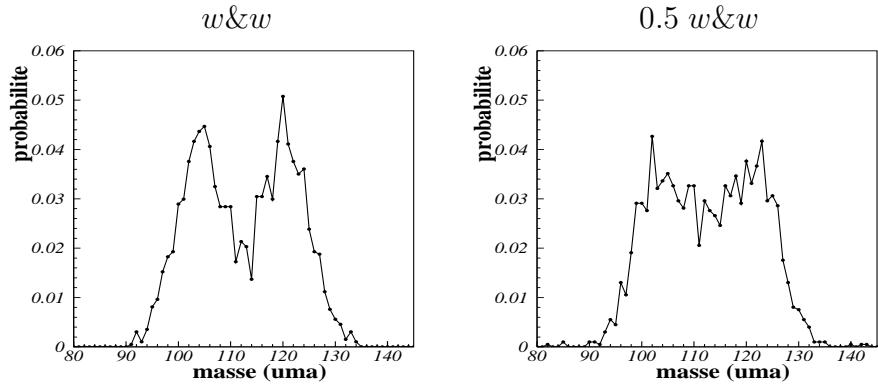


FIG. 12. Fission-fragment mass distributions obtained for the system ^{227}Pa ($E_{\text{tot}}^* = 56$ MeV, $L = 60\hbar$) with the full ($w\&w$) and a reduced ($0.5 w\&w$) friction (see text).

5. Confrontation with experimental data

As the agreement theory-experiment at high excitation energy is quite promising [19], we would like to compare in the present section our predictions to the available experimental data concerning the fission process of

the nucleus ^{227}Pa synthesized at a total excitation energy of $E_{tot}^* = 26$ MeV [21]. In the calculations we should obviously take particle evaporation into account. Since we do not have for the moment a complete reliable evaporation theory at our disposal at low temperature we first performed dynamical calculations at higher energy for which we believe that the Weisskopf's approach is about reasonable. This study showed us that the influence of particle evaporation on the fission fragment mass distribution can be neglected [21]. As the probability of emitting particles decreases with excitation energy [5], we also expect a really small impact of evaporation on the mass distribution at 26 MeV. Consequently we compare in Fig. 13 mass distributions obtained for $E_{tot}^* = 26$ MeV without taking evaporation into account with the experimental mass distribution. We have considered in the theoretical calculations three different frictions : 25% of the wall and window value, 20% and 15%.

The experimental analysis has exhibited a multi-modal fission-fragment mass distribution [21] composed of three modes : the symmetric one and two asymmetric modes centered around mass $A = 132$ corresponding to the double magic ^{132}Sn nucleus and around mass $A = 140$ related to the deformed ^{140}Ba nucleus, explained [32, 33] by the closure of the deformed neutron shell $N = 84$. The comparison with our predictions shows that in the case of a friction corresponding to 15% of the wall-and-window value the model reproduces quite well the symmetric fission mode. We would like to mention here that microscopic calculations performed by Hofmann and Ivanyuk [34] indicate that such a reduced viscosity is about what is to be expected at such low excitation energy. However our calculation gives only rise to the asymmetric $A=132$ channel, the $A = 140$ mode being absent.

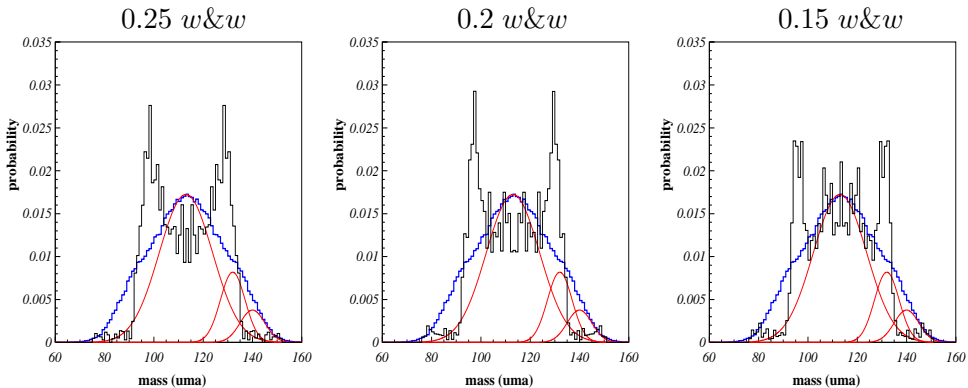


FIG. 13. Experimental (solid line) and theoretical (histograms) fission fragment mass distributions for the system ^{227}Pa ($E_{tot}^* = 26$ MeV) for different values of the friction.

In order to understand the disagreement between our model and the experimental data for asymmetric fission we have to remember that we have chosen to describe nuclear shapes in the 2-dimensional deformation space (c, α) imposing $h=0$. Taking h different from zero will allow us to consider a larger variety of nuclear configurations. We thus believe that with the restricted 2-dimensional parametrization we are not able to give a description of the deformed shape of ^{140}Ba but that when taking $h \neq 0$ into account we will describe that shape and the corresponding asymmetric fission valley so that a part of the trajectories which, for $h=0$, end up in the $A=132$ channel will reach, in the case of $h \neq 0$, the previously missing $A=140$ valley. The contribution to the fission mode $A=132$ will then decrease while the one of the $A=140$ channel will increase, thus reaching a better agreement between theory and experiment when we will have extended the present 2-dimensional treatment to a 3-dimensional one. Investigations along this direction are under way.

6. Discussion and conclusions

With the purpose to study multi-modal fission, we have developed a model describing the dynamics of the fission process by the resolution of a 2-dimensional Langevin equation coupled to the Master equations governing particle emission. Starting from a more or less classical description proven as rather successful for describing symmetric fission at high excitation energy, we extended our theory to multi-modal fission by increasing the dimensionality of the deformation space in which the Langevin equation is solved in order to be able to deal with asymmetric shapes and by including quantal effects (shell and pairing corrections) in the potential-energy calculations. Our investigations show the strong sensitivity of the dynamics on the structure of the potential-energy landscape what implies the necessity for a careful description of the later, in particular in the determination of shell and pairing corrections at large deformation.

Comparing theoretical and experimental fission-fragment mass distributions one observes a rather promising agreement which, as we believe, could still be considerably improved if the 2-dimensional treatment is extended to a 3-dimensional one. We also point out the importance of taking into account the temperature dependence of nuclear friction which as we have seen should be significantly reduced at low energy. Another crucial aspect of the problem lies in the necessity of a reliable evaporation theory at low excitation energy.

Up to now the general analysis was that pre-scission light-particle multiplicities were the quantities to investigate [6, 19] for a better understanding of fission dynamics. Our present study shows, on the contrary, that at low

excitation energies where the number of emitted particles is small and, in the frequent case where the competition between symmetric and asymmetric channels exhibits multi-modal fission, the fragment mass distribution is probably more relevant, in particular for investigating transport coefficients like nuclear friction.

Acknowledgments

Two of us (C.S. and J.B.) are very grateful for the hospitality extended to them on many occasions by the Theory Department of the Marie-Curie-Skłodowska University in Lublin. A.S. and K.P. are in turn very thankful for many fruitful visits they were able to do to the Strasbourg Nuclear Research Center IReS and its Nuclear Theory group. K.P. especially acknowledges a PAST position granted to him by the University Louis Pasteur and the French Ministry of National Education and Research. This work was partially sponsored by the Polish Committee of Scientific Research KBN No. 2P 03B 115 19 and the POLONIUM fellowship No. 007/IN2P3/4788/2002.

REFERENCES

- [1] P. Grangé, H.C. Pauli and H.A. Weidenmüller, Phys. Lett. **B88** (1979) 9; Z. Phys. **A296** (1980) 107.
- [2] E. Strumberger, W. Dietrich and K. Pomorski, Nucl. Phys. **A529** (1991) 522.
- [3] W. Przystupa, K. Pomorski, Nucl. Phys. **A572** (1994) 153.
- [4] Y. Abe, S. Ayik, P.-G. Reinhard and E. Suraud, Phys. Rep. **275** (1996) 49.
- [5] K. Pomorski, J. Bartel, J. Richert and K. Dietrich, Nucl. Phys. **A605** (1996) 87.
- [6] P. Fröbrich, I.I. Gontchar, Phys. Rep. **292** (1998) 131.
- [7] K. Pomorski, E. Strumberger, Ann.Univ.MCS, Poland, sec.AAA XLV (1990) 113.
- [8] S. Trentalange, S.E. Koonin, A. Sierk, Phys. Rev. **C22** (1980) 1159.
- [9] M. Brack, J. Damgaard, A.S. Jensen, H.C. Pauli, V.M. Strutinsky, C.Y. Wong, Rev. Mod. Phys. **44** (1972) 320.
- [10] K.T.R. Davies, A.J. Sierk, J.R. Nix, Phys. Rev. **13C** (1976) 2385.
- [11] J. Blocki, J. Randrup, W. J. Swiatecki and C.W. Tsang, Ann. Phys. **105** (1977) 427.
- [12] H. Feldmeier, Rep. Prog. Phys. **50** (1987) 915.
- [13] J. Bartel, K. Mahboub, J. Richert and K. Pomorski, Z. Phys. **A354** (1996) 59.
- [14] K. Pomorski, H. Hofmann, Phys. Lett. **B263** (1991) 164.

- [15] H. Hofmann, F.A. Ivanyuk, Phys. Rev. Lett. **82** (1999) 4603.
- [16] V.M. Strutinsky, Nucl. Phys. **A95** (1967) 420; **A122** (1968) 1.
- [17] J. Bardeen, L.N. Cooper and J.R. Schrieffer, Phys. Rev. **108** (1957) 1175.
- [18] S.G. Nilsson, C.F. Tsang, A. Sobiczewski, Z. Szymanski, S. Wycech, C. Gustafson, I.-L. Lamm, P. Moller, B. Nilsson, Nucl. Phys. **A131** (1969) 1.
- [19] K. Pomorski, B. Nerlo-Pomorska, A. Surowiec, M. Kowal, J. Bartel, K. Dietrich, J. Richert, C. Schmitt, B. Benoit, E. de Goes Brennand, L. Donadille, C. Badimon, Nucl. Phys. **A679** (2000) 25.
- [20] C. Schmitt, A. Surowiec, J. Bartel, K. Pomorski, Proceedings of the Int. Conf. Nuclear Physics at Border Lines, Lipari, Italy, May 21-24, 2001, Edited by G.Fazio, G.Giardina, F.Hanappe, G.Imm and N.Rowley, World Scientific.
- [21] C. Schmitt, PhD Thesis, Université Louis Pasteur Strasbourg (2002), IReS 02 – 04.
- [22] V. Weisskopf, Phys. Rev. **52** (1937) 295.
- [23] K. Dietrich, K. Pomorski and J. Richert, Z. Phys. **A351** (1995) 397.
- [24] A. Surowiec, K. Pomorski, C. Schmitt, Acta Physica Polonica **B33** (2002). in Nuclear Fission, Contributed Papers, W. Berlin (1989), 63.
- [25] A.V. Ignatyuk, Phys. Lett. **B76** (1978) 543.
- [26] A.V. Ignatyuk, Nucl. Phys. **A346** (1980) 191.
- [27] A.V. Ignatyuk, G.N. Smirenkin, A.S. Tishin, Yad. Fiz. **21** (1975) 485.
- [28] J.L. Egido, L.M. Robledo, V. Martin, Phys. Rev. Lett. **85** (2000) 054308.
- [29] P. Moller, S.F. Nilsson, Phys. Lett. **B31** (1970) 283.
- [30] J.M. Maruhn, W. Greiner, Phys. Rev. Lett. **32** (1974) 548.
- [31] B. Nerlo-Pomorska, K. Pomorski, E. Werner, International Conference Fifty Years Research
- [32] U. Brosa, S. Grossman, A. Muller, Physics Reports, **197** (1990) 167.
- [33] I.V. Pokrovsky et al., Phys. Rev. **C62** (2000) 014615.
- [34] H. Hofmann, F.A. Ivanyuk, C. Rummel, S. Yanji, Phys. Rev. **C64** (2001) 054316.